Magnetization Transfer Imaging Is Unaffected by Decreases in Renal Perfusion in Swine

Kai Jiang, PhD, Christopher M. Ferguson, MS,* John R. Woollard, MS,* Vanessa L. Landes, BS,† James D. Krier, MS,* Xiangyang Zhu, MD, PhD,* Krishna S. Nayak, PhD,† and Lilach O. Lerman, MD, PhD**

Objectives: Multiparametric renal magnetic resonance imaging (MRI), including diffusion-weighted imaging, magnetic resonance elastography, and magnetization transfer imaging (MTI), is valuable in the noninvasive assessment of renal fibrosis. However, hemodynamic changes in diseased kidneys may impede their ability to measure renal fibrosis. Because MTI assesses directly tissue content of macromolecules, we test the hypothesis that MTI would be insensitive to renal hemodynamic changes in swine kidneys with acute graded ischemia.

Materials and Methods: Seven domestic pigs underwent placement of an inflatable silicone cuff around the right renal artery to induce graded renal ischemia. Multiparametric MRI was performed at baseline, 50%, 75%, and 100% renal artery stenosis as well as reperfusion. Measurements included regional perfusion, R_2*, apparent diffusion coefficient (ADC), stiffness, and magnetization transfer ratio (MTR) using arterial spin-labeled MRI, blood oxygenation–dependent MRI, diffusion-weighted imaging, magnetic resonance elastography, and MTI, respectively. Histology was performed to rule out renal fibrosis.

Results: During graded ischemia, decreases in renal perfusion were accompanied with elevated R_2*, decreased ADC, and stiffness, whereas no statistically significant changes were observed in the MTR. No fibrosis was detected by histology. After release of the obstruction, renal perfusion showed only partial recovery, associated with return of kidney R_2*, ADC, and stiffness to baseline levels, whereas cortical MTR decreased slightly.

Conclusions: Renal MTI is insensitive to decreases in renal perfusion and may offer reliable assessment of renal structural changes.

Key Words: renal fibrosis, magnetic resonance imaging, diffusion-weighted imaging, magnetic resonance elastography, magnetization transfer imaging

(*Invest Radiol* 2019;54: 681–688)

Chronic kidney disease (CKD) is a worldwide health issue, afflicting around 14% of the population.[1] Chronic kidney disease is progressive and may eventually lead to end-stage renal disease, a devastating disorder that requires renal transplant therapy and imposes great cost to both the individual and society. Early and reliable diagnosis of CKD is imperative for timely and optimal management to prevent disease progression. Renal fibrosis is the final common pathway of CKD and serves as an important biomarker in the diagnosis of renal diseases as well as evaluation of therapeutic interventions.[2] The current criterion standard method for evaluation of renal fibrosis is percutaneous renal biopsy, which is limited by its invasiveness, incomplete sampling coverage, and potential complications.[3]

Recent advances in renal magnetic resonance imaging (MRI) have shown promise for noninvasive assessment of renal fibrosis by assessing its impact on the functional, mechanical, and molecular properties of the kidney. Diffusion-weighted imaging (DWI) can be used to measure tissue water mobility characterized by the apparent diffusion coefficient (ADC), which is considered to fall secondary to deposition of extracellular matrix in fibrotic kidneys. Extracellular matrix deposition leading to scarring typically stiffens affected organs.[4] Therefore, tissue stiffness measured using magnetic resonance elastography (MRE) has been used as an index of fibrosis. At the molecular level, a fibrotic kidney is featured by elevated macromolecule content due to accumulation of extracellular matrix components, composed mainly of fibronectin and collagen type I, III, and IV.[5] Such increased macromolecule content serves as an important biomarker for renal fibrosis and can be assessed using magnetization transfer imaging (MTI).

The utility of these MRI techniques for measuring renal fibrosis has been demonstrated in previous studies. Significant negative correlations between the ADC and renal fibrosis have been reported in both preclinical animal models[6–9] and patients,[10–12] supporting the usefulness of the ADC in noninvasive measurement of renal fibrosis. Nevertheless, decrease in the ADC in fibrotic kidneys is attributable to not only restricted true water diffusion but also lower microvascular perfusion and tubular flow.[13,14] Similarly, kidney stiffness drops due to decreased tissue turgor resulting from renal hypoperfusion,[15] which offsets the effect of renal fibrosis on tissue stiffness.[16] The anisotropic structure of renal tissue has also been shown to influence tissue stiffness.[17] Therefore, the usefulness of DWI and MRE in measuring renal fibrosis might be compromised by lower renal perfusion.

Recently, MTI has emerged as a promising technique for measurement of renal fibrosis. Magnetization transfer is a physical phenomenon that describes the cross relaxation between water molecules bound to macromolecules (the bound pool) and free water molecules (the free pool). In MRI, the macromolecules cannot be directly measured due to their extremely short T_2 (<1 millisecond).[18] Nonetheless, saturation of the bound pool with off-resonance MT pulses induces a decrease in the free pool MR signal because of the MT between these 2 pools. The percent change in the detected MR signal, or MT ratio (MTR), reflects the content of macromolecules and has recently been shown to correlate well with ex vivo renal fibrosis by histology.[19–22] Notably, because the MTR is dependent on tissue macromolecule content, MTI, compared with other MRI techniques, may be less sensitive to alterations in renal hemodynamics.

Therefore, in this study, we aimed to test the hypothesis that MTI is insensitive to decreases in renal perfusion. The impact of renal perfusion on MTI was evaluated in swine kidneys with graded ischemia. To compare MTI with other MRI techniques, changes in renal perfusion, water diffusion, and stiffness were also evaluated using arterial spin labeling (ASL), DWI, and MRE, respectively. In addition, renal oxygenation was assessed by blood oxygenation–dependent (BOLD) MRI. Finally, renal histology was performed to exclude the presence of renal fibrosis in this acute model.

Received for publication April 4, 2019; and accepted for publication, after revision, May 9, 2019.

From the *Division of Nephrology and Hypertension, Mayo Clinic, Rochester, MN; and †Ming Hsieh Department of Electrical and Computer Engineering, Viterbi School of Engineering, University of Southern California, Los Angeles, CA.

Conflicts of interest and sources of funding: No conflicts of interest were declared. This study was partly supported by the National Institutes of Health grants DK104273, DK102325, DK120292, HL123160, HL130494, and C06-RR018898.

Correspondence to: Lilach O. Lerman, MD, PhD, Division of Nephrology and Hypertension, Mayo Clinic College of Medicine, 200 First St SW, Rochester, MN 55905. E-mail: Lerman.Lilach@mayo.edu.

ISSN: 0020-9996/19/5411–0681
DOI: 10.1097/RLI.0000000000000588

MATERIALS AND METHODS

Animal Preparation

All animal experiments were approved by the Institutional Animal Care and Use Committee in our institution. Seven 3-month-old female domestic pigs (*Sus scrofa*; Manthei Hog Farm LLC, Elk River, MN) were used. Anesthesia of animals was maintained with 1% to 2% isoflurane during surgery and MRI. Endotracheal intubation was performed for mechanical ventilation and ear-vein catheterization for saline infusion (5 mL/min). To restrict renal blood flow and induce graded renal ischemia, an inflatable MR-compatible silicone cuff (DocXS Biomedical Products & Accessories, Ukiah, CA) was placed around the right renal artery, after a small flank incision. The cuff was first calibrated for various degrees of renal artery stenosis (RAS, dictated by cuff diameter) by injection of saline. After the placement of the cuff, the animal was prepared for MRI.

MRI Study

All MRI studies were performed on a GE Signa HDxt 3.0 T scanner (GE Healthcare, Waukesha, WI). The body coil was used as the transmitter and an 8-channel surface coil used as the receiver. Kidney imaging was performed first at baseline, then 50%, 75%, and 100% RAS by inflating the renal artery cuff using cumulative amounts of saline, and finally recovery after release of the cuff. A 5-minute resting period between different grades of RAS was maintained for hemodynamic stabilization before the next iteration of MRI examination. Multiparametric MRI was used to successively measure renal perfusion, R_2*, MTR, stiffness, and diffusion in this order in all animals. To avoid respiratory motion artifacts, all MRI scans were performed with suspended respiration. A complete set of MRI scans took approximately 50 minutes, resulting a total imaging time of approximately 4 hours per animal.

Renal perfusion was measured by ASL using a FAIR-SSFP (flow-sensitive alternating inversion recovery labeling and transient balanced steady-state free precession) imaging sequence.[23–25] One 10-mm axial slice was imaged at the kidney hilum, from which 12 control and tagged image pairs were obtained. A hyperbolic secant adiabatic pulse was used for magnetization inversion. Slice-selective inversion was performed on a 30-mm slab to achieve uniform inversion of the imaging slice. Other imaging parameters were as follows: repetition time (TR), 3.0 milliseconds; echo time (TE), 1.5 milliseconds; field of view (FOV), 30 × 30 cm^2, matrix size, 128 × 128; and inversion delay, 1.2 seconds.

Renal oxygenation was assessed by BOLD-MRI using a multiecho gradient echo sequence. A total of 16 images with echo times from 3.5 to 63.5 milliseconds were acquired per slice. Other imaging parameters were as follows: TR, 200 milliseconds; flip angle, 40 degrees; slice number, 5; slice thickness, 2.6 mm; FOV, 30 × 30 cm^2; matrix size, 192 × 128; and number of excitations, 1.

Kidney MTR was measured using an MT-prepared gradient echo (GRE) sequence. Images without MT pulses were acquired in the coronal plane with the following parameters: TR, 300 milliseconds; TE, 5.3 milliseconds; flip angle, 30 degrees; slice thickness, 2.6 mm; slice number, 5; FOV, 30 × 30 cm^2; matrix size, 192 × 128; phase field of view, 0.75; and number of excitations, 1. Then MT-weighed images were acquired by adding Fermi pulses before GRE acquisition. The MT pulse parameters were as follows: offset frequency, both 600 and 1000 Hz; pulse width, 16 milliseconds; and flip angle, 800 degrees.

Kidney stiffness was measured by MRE using a spin-echo echo-planar imaging sequence with motion sensitizing gradients and flow compensation. As described previously,[15] shear waves (120 Hz vibrations) were transmitted to the kidneys by placing 2 passive pneumatic drivers under each kidney on the posterior of the body. A total of 48 axial slices were acquired to cover the entire kidneys. Other imaging parameters were as follows: TR, 2200 milliseconds; TE, 65 milliseconds; FOV, 35 × 35 cm^2; matrix size, 96 × 96; and slice thickness, 2.5 mm. For corticomedullary segmentation, T_1-weighted images of the same slices were acquired using the GRE sequence with the following parameters: TR, 200 milliseconds; TE, 5.6 milliseconds; matrix size, 256 × 192; and flip angle, 45 degrees.

Kidney diffusion was measured by DWI using a single-shot spin-echo echo-planar imaging sequence. Diffusion-weighted images were acquired from 4 to 6 coronal slices. Two relatively high b-values at 600 and 1000 s/mm^2 were selected to minimize the impact of reduced blood flow on measured ADC.[26] Other imaging parameters were TR, 1800 milliseconds; TE, 51.8–101.5 milliseconds; FOV, 35 × 35 cm^2; matrix size, 128 × 128; and slice thickness, 2.6 cm.

Image Analysis

Renal elastograms were generated by postprocessing wave images using a multimodel direct inversion algorithm (MMDI).[27,28] Briefly, the MMDI algorithm uses a multitude of polynomial fits and utilizes a statistical F test that aids in selection of the optimal fit. Removal of longitudinal waves was achieved with MMDI by using the total least squares, satisfying the Helmholtz equation in the remaining shear waves. The cortical and medullary regions of interest were defined on the T_1-weighted images and propagated onto the elastograms to calculate stiffness.[15]

All other image analysis was performed using software modules developed in-house in Matlab (Mathworks, Natick, MA). Renal cortical perfusion map was generated from the difference image of the tagged and nontagged images, as described previously.[23] To calculate renal perfusion, cortical and medullary T_1 values of 1.3 and 1.6 seconds were used for all animals.[29] Kidney T_2* was calculated by monoexponential fitting of the BOLD images with different echo times and R_2* as $1/T_2$*. The MTR was calculated as the percentage signal decrease from baseline to MT-weighted images, and then normalized by MTR of the ipsilateral psoas muscle major to correct for B_1 variations.[22] Kidney ADC maps were generated by pixel-wise monoexponential fitting of the diffusion-weighted images. Cortical and medullary regions of interest for BOLD-MRI, MTI, and DWI were selected on T_2*-weighted images using a semiautomated image segmentation algorithm.[22] For measurement of renal R_2* and ADC, kidney regions with susceptibility artifact were excluded to avoid biased estimation.

Ex Vivo Studies

After MRI, pigs were euthanized with kidneys harvested and fixed in 10% formalin. Trichrome staining was performed on 5-μm-thick kidney sections to evaluate the presence of renal fibrosis, in comparison to normal kidneys of matched pigs.

Statistical Analysis

Statistical analysis was performed using JMP 14.0 (SAS Institute, Cary, NC). All results were expressed as means ± standard deviations. One-way analysis of variance followed by paired t test was performed to compare all renal parameters at different time points. Statistical significance was judged at $P < 0.05$.

RESULTS

All experimental pigs had similar body weight (54.1 ± 2.5 kg). Representative cortical perfusion maps overlaid on anatomical images acquired at baseline, graded ischemia, and recovery are shown in Figure 1A. The cortical perfusion decreased substantially from baseline to all degrees of RAS (Fig. 1B, Table 1; $P < 0.001$). After the release of the cuff, cortical perfusion showed mild recovery compared with full occlusion ($P = 0.045$), but remained lower than at baseline ($P = 0.001$). Similar decreases in the medullary perfusion were also observed at graded ischemia (50% RAS, $P = 0.003$; 75% and 100% RAS, $P < 0.001$), as compared with baseline. At recovery, the

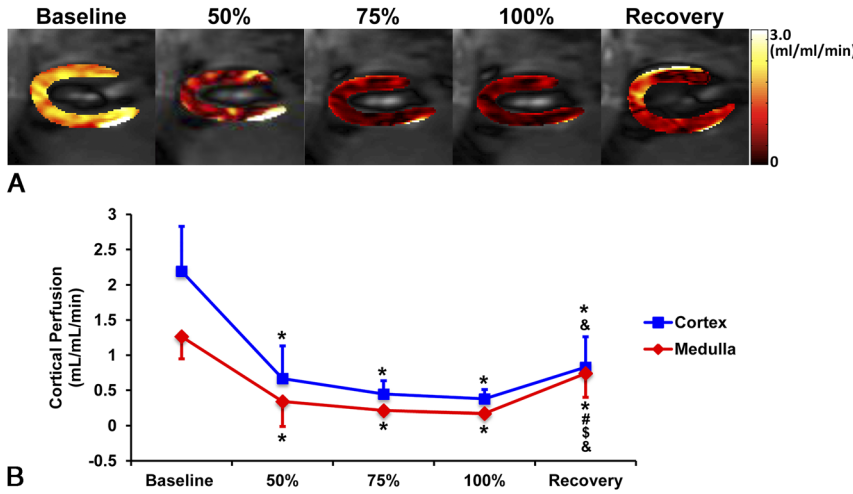

FIGURE 1. Kidney perfusion by arterial spin labeling. A, Representative cortical perfusion maps (overlaid on anatomical images) acquired at baseline, graded ischemia, and recovery. B, Cortical and medullary perfusion measured at all time points. *$P < 0.05$ vs baseline, #$P < 0.05$ vs 50% RAS, $$P < 0.05$ vs 75% RAS, &$P < 0.05$ vs 100% RAS.

medullary perfusion rose significantly compared with all degrees of RAS ($P = 0.027$ vs 50% RAS; $P = 0.009$ vs 75% RAS; $P = 0.004$ vs 100% RAS), but remained slightly lower than at baseline ($P = 0.019$).

Representative renal R_2* maps overlaid on anatomical images acquired at baseline, graded RAS, and recovery are shown in Figure 2A. Similar changes in renal R_2* were observed in the renal cortex and medulla throughout the study. Significant renal hypoxia developed at 50% RAS compared with baseline, as indicated by a rise in both cortical (Fig. 2B, Table 1; $P = 0.008$) and medullary ($P = 0.003$) R_2*. Increasing constriction of the renal artery led to higher R_2* at 75% (cortex, $P = 0.011$; medulla, $P < 0.001$) and 100% (cortex, $P = 0.010$; medulla, $P < 0.001$) RAS. At recovery, kidney reperfusion abolished tissue hypoxia, as demonstrated by normalized cortical and medullary R_2*.

Shown in Figure 3A are representative renal elastograms at all time points. Renal cortical and medullary stiffness showed similar changes in response to the graded ischemia and reperfusion. Compared with baseline, renal stiffness at 50% (Fig. 3B, Table 1; cortex, $P = 0.003$; medulla, $P = 0.005$), 75% (cortex, $P = 0.008$; medulla,

TABLE 1. Renal Changes During Acute Renal Ischemia and Recovery by Multiparametric MRI

	Baseline	50% RAS	75% RAS	100% RAS	Recovery
Perfusion, mL/mL/min					
Cortex	2.19 ± 0.63	0.67 ± 0.47*	0.45 ± 0.19*	0.38 ± 0.13*	0.83 ± 0.43*§
Medulla	1.26 ± 0.32	0.34 ± 0.35*	0.21 ± 0.05*	0.17 ± 0.03*	0.74 ± 0.39*†‡§
R_2*, s^{-1}					
Cortex	17.8 ± 1.8	31.2 ± 9.4*	50.6 ± 13.6*†	57.1 ± 18.1*†	19.5 ± 6.9†‡§
Medulla	20.2 ± 2.5	41.8 ± 13.4*	64.1 ± 13.3*†	67.2 ± 13.5*†	19.1 ± 3.7†‡§
Stiffness, kPa					
Cortex	4.76 ± 0.49	3.72 ± 0.34*	3.79 ± 0.47*	3.66 ± 0.57*	6.19 ± 1.46†‡§
Medulla	4.54 ± 0.53	3.59 ± 0.20*	3.46 ± 0.39*	3.40 ± 0.42*	5.31 ± 0.97†‡§
ADC, $\times 10^{-3}$ mm^2/s					
Cortex	1.54 ± 0.21	0.94 ± 0.22*	0.87 ± 0.18*	0.82 ± 0.19*	1.41 ± 0.07†‡§
Medulla	1.51 ± 0.23	0.99 ± 0.19*	0.94 ± 0.16*	0.95 ± 0.15*	1.51 ± 0.16†‡§
MTR at 600 Hz					
Cortex	0.81 ± 0.03	0.81 ± 0.05	0.80 ± 0.04	0.79 ± 0.04	0.77 ± 0.03*†
Medulla	0.75 ± 0.04	0.76 ± 0.05	0.77 ± 0.04	0.75 ± 0.03	0.73 ± 0.05
MTR at 1000 Hz					
Cortex	0.76 ± 0.03	0.78 ± 0.06	0.76 ± 0.04	0.74 ± 0.04	0.64 ± 0.05*†
Medulla	0.67 ± 0.03	0.71 ± 0.05	0.71 ± 0.02	0.69 ± 0.04	0.73 ± 0.05

Data are means ± standard deviations.

*$P < 0.05$ vs baseline.

†$P < 0.05$ vs 50% RAS.

‡$P < 0.05$ vs 75% RAS.

§$P < 0.05$ vs 100% RAS.

MRI indicates magnetic resonance imaging; RAS, renal artery stenosis; ADC, apparent diffusion coefficient; MTR, magnetization transfer ratio.

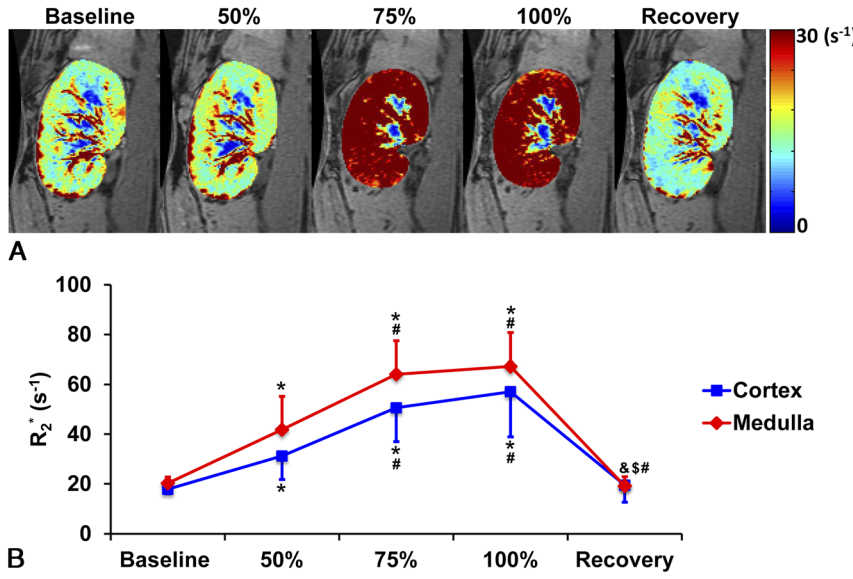

FIGURE 2. Renal oxygenation by blood oxygenation level–dependent MRI. A, Representative kidney R_2* maps at baseline, graded ischemia, and recovery. Increasing intensity and extent of the red color suggests development of hypoxia. B, R_2* measured in the renal cortex and medulla at all time points. *$P < 0.05$ vs baseline, #$P < 0.05$ vs 50% RAS, $$P < 0.05$ vs 75% RAS, &$P < 0.05$ vs 100% RAS.

$P = 0.003$), and 100% (cortex, $P = 0.008$; medulla, $P = 0.001$) RAS all significantly decreased. After renal reperfusion, both cortical and medullary stiffness rose above those at all degrees of RAS, and tended to increase (cortex, $P = 0.063$; medulla, $P = 0.069$) compared with their basal values.

Representative renal ADC maps are shown in Figure 4A. The whole kidney parenchyma showed similar changes in ADC in response to different degrees of renal ischemia. Similar to renal stiffness, the cortical ADC, compared with baseline, dropped substantially at all levels of RAS (Fig. 4B, Table 1; $P < 0.001$), and completely recovered after release of the cuff ($P < 0.05$ compared with all levels of RAS). Similar changes in the medullary ADC were also observed at graded ischemia ($P < 0.001$), as compared with baseline. At recovery, the medullary ADC rose significantly compared with all degrees of RAS ($P < 0.001$), and returned to the basal level.

Representative kidney MTR maps overlaid on anatomical images acquired at different time points are shown in Figure 5A. Unlike all aforementioned renal parameters, cortical and medullary MTR at 600 Hz remained unchanged from baseline to all levels of RAS (Fig. 5B, left; Table 1). A mild but significant decrease was observed in cortical MTR at recovery, as compared with baseline ($P = 0.013$) and 50% RAS ($P = 0.026$), although it was not different from 75% and 100% obstruction. Similar changes in cortical and medullary MTR were observed with the MT offset frequency set at 1000 Hz (Fig. 5B, right; Table 1).

Trichrome-stained cortical and medullary tissue sections showed no renal fibrosis in any experimental kidney (Fig. 6). However, some

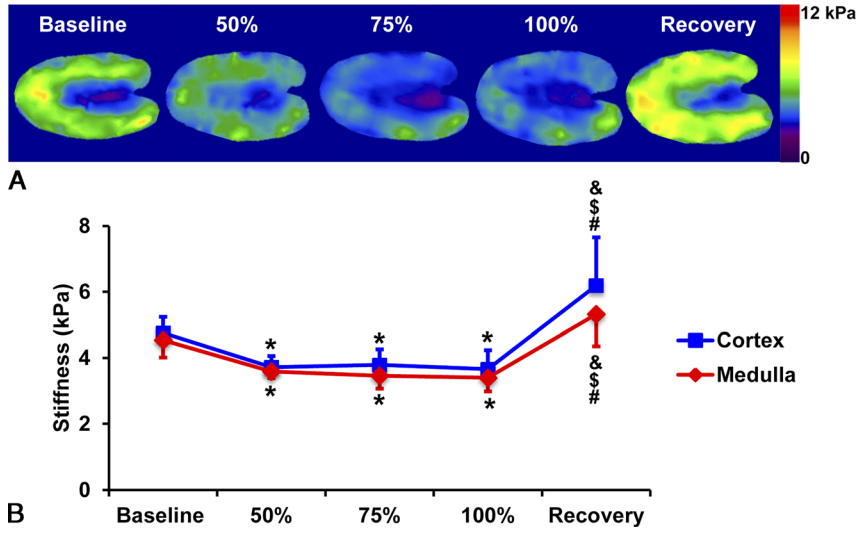

FIGURE 3. Kidney stiffness by magnetic resonance elastography. A, Representative kidney elastograms at baseline, graded ischemia, and recovery. B, Cortical and medullary stiffness measured at all time points. *$P < 0.05$ vs baseline, #$P < 0.05$ vs 50% RAS, $$P < 0.05$ vs 75% RAS, &$P < 0.05$ vs 100% RAS.

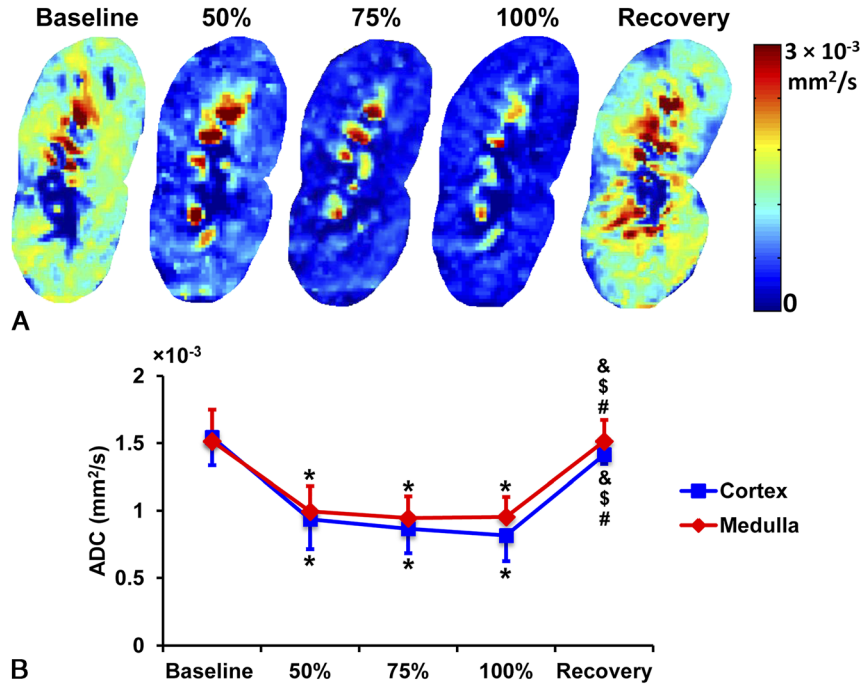

FIGURE 4. Renal apparent diffusion coefficient by diffusion-weighted imaging. A, Representative kidney ADC maps at baseline, graded ischemia, and recovery. B, Kidney parenchymal ADC measured at all time points. $^{*}P < 0.05$ vs baseline, $^{\#}P < 0.05$ vs 50% RAS, $^{\$}P < 0.05$ vs 75% RAS, $^{\&}P < 0.05$ vs 100% RAS.

evidence of acute kidney injury was observed, including enlarged Bowman's space, tubular dilation, and inflammatory infiltration.

DISCUSSION

In this study, we show that MTI-measured MTR is unaffected by decreases in renal perfusion during graded ischemia in swine kidneys. By contrast, renal stiffness by MRE and ADC by DWI dropped substantially, despite no development of renal fibrosis. Those changes were accompanied by elevated tissue R_2*, that is, hypoxia as measured by BOLD-MRI. Subsequent tissue reperfusion normalized kidney stiffness, ADC, and R_2*, although renal perfusion remained lower than baseline, possibly as a result of ischemia-reperfusion injury, whereas the cortical MTR slightly rose.

Renal fibrosis is closely related to chronic changes in renal function[30,31] and has been widely used in diagnosis of renal diseases, prediction of renal outcome in CKD[32,33] or transplant status,[34–36] and

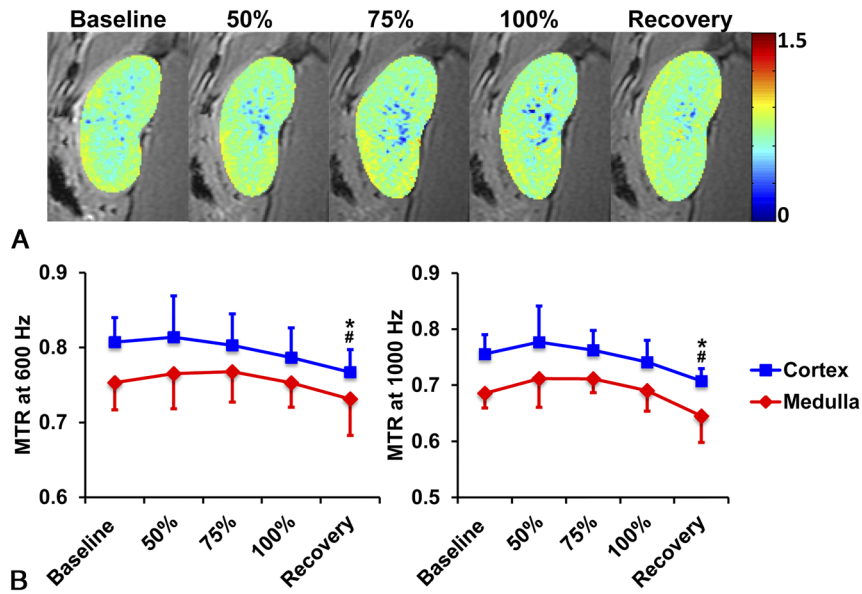

FIGURE 5. Kidney magnetization transfer ratio (MTR) by MTI. A, Representative kidney MTR maps acquired with the MT offset frequency at 600 Hz. B, Cortical and medullary MTR quantified with the MT offset frequency at 600 (left) and 1000 (right) Hz at baseline, graded ischemia, and recovery. $^{*}P < 0.05$ vs baseline, $^{\#}P < 0.05$ vs 50% RAS.

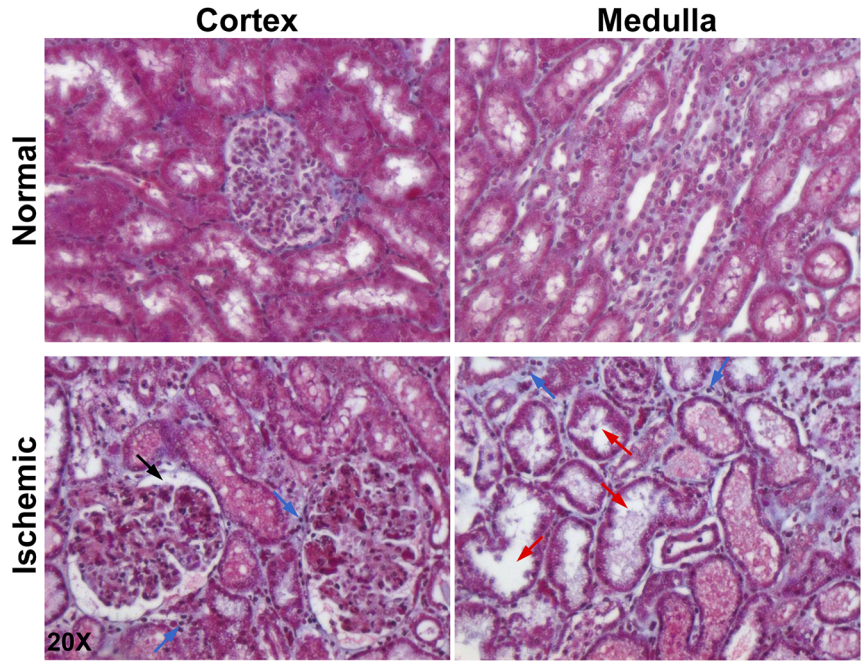

FIGURE 6. Kidney injuries post graded ischemia and reperfusion. Representative trichrome-stained cortical and medullary tissue sections from normal and ischemic kidneys. No renal fibrosis was detected in either cortex or medulla of pig kidneys with graded ischemia. However, signs of acute kidney injury were observed, including enlarged Bowman's space, tubular dilation, and inflammatory infiltration as marked by arrows with black, red, and blue colors, respectively.

assessment of therapies.[37–40] Although renal biopsy is the reference standard method for fibrosis assessment, it is fraught with limitations. Noninvasive and reliable assessment of renal fibrosis would be of great value in clinical practice and research, and has greatly fueled investigators' efforts in developing novel fibrosis imaging techniques. Recent advances in MR renal imaging provide exciting opportunities for noninvasive assessment of renal fibrosis. MRI techniques such as DWI, MRE, and MTI offer new opportunities for noninvasive measurement of renal fibrosis by assessing its impact on the kidney. Yet, concurrent alterations in hemodynamics of dysfunctional kidneys constitute a confounding element that may hamper the reliability of MRI techniques in fibrosis assessment. Swine kidneys with graded renal ischemia and no detectable renal fibrosis provide a good model to elucidate the direct effect of renal hemodynamics on these MRI techniques.

In nonfibrotic ischemic kidneys, reduction in perfusion was accompanied by a substantial decrease in kidney ADC, despite the use of high b-values greater than 600 s/mm^2 to minimize the effect of perfusion on measured ADC.[26] In line with our findings, Prasad et al[41] observed a significant correlation between the cortical ADC derived from b-values ranging from 200 to 1000 s/mm^2 and ASL-measured perfusion in CKD patients. The fall in ADC may be attributed to the tubular compartment, which introduces a third intermediate diffusion component in the kidney,[14] because a reduction in renal blood flow can in turn decrease tubular volume,[42] and thereby lower water diffusion and ADC. Therefore, a drop in renal perfusion may limit the specificity of the ADC in serving as a true index of renal fibrosis.[43] Pertinently, one study reported that the cortical ADC decreased in vivo but increased at postmortem due to tubular dilation and expanded extracellular space in rat fibrotic kidneys with unilateral ureteral obstruction.[43] In addition, we have also shown that excessive renal fat may lead to underestimation of renal ADC, compromising its utility in detection of renal pathology.[44] Taken together, the in vivo ADC is notably dependent on renal hemodynamics as well as fat content, limiting its sensitivity to renal fibrosis.

Similar to the ADC, MRE-measured renal stiffness also dropped substantially during graded ischemia, possibly due to a fall in perfusion pressure. This is consistent with previous findings in a similar swine model[15] and in patients with lupus nephritis,[45] and in line with the impact of renal perfusion on stiffness using ultrasound elastography.[46,47] Indeed, renal stiffness is dependent on a number of factors other than renal fibrosis, including tissue perfusion pressure, tubular or interstitial pressure, and tissue anisotropy.[17] Changes in these factors may offset the effect of fibrosis in stiffening the kidney. As a result, MRE has been shown to be unreliable in assessing cortical fibrosis during a fall in renal blood flow.[16]

Unlike other MRI techniques, MTI provides unique tissue contrast that is indicative of the macromolecule content, which serves as a useful biomarker for renal fibrosis. Notably, the capability of MTI in measuring renal fibrosis has been demonstrated by a good spatial concordance between the MTR map and histological sections as well as by its good correlation with the degree of fibrosis.[20] Yet, it remained unclear whether factors other than renal fibrosis, such as lower renal perfusion, could contribute to the increased MTR. In this study, we extend our previous findings and demonstrate the relative insensitivity of MTI to alterations in renal hemodynamics, as supported by the unchanged MTR at different degrees of RAS. Therefore, MTI may offer a reliable tool for assessing renal fibrosis, regardless of renal hemodynamic hypoperfusion.

Kidney reperfusion after releasing the renal artery cuff caused differential levels of recovery of the measured MRI parameters. The prolonged ischemia during the experimental protocol followed by reperfusion-induced detectable kidney changes, including enlarged Bowman's space, tubular dilation, and inflammatory infiltration. These tissue injuries might have led to an incomplete recovery of renal perfusion after releasing the renal artery obstruction. On the other hand, we observed a slight drop in cortical MTR after reperfusion. Previous studies have shown that acute kidney injury results in short-term activation of proteases that lead to a decrease in laminin and

collagen.[48,49] By contrast, renal oxygenation, stiffness, and water diffusion all fully recovered to basal levels. Importantly, the divergent findings by these MRI techniques at recovery underscore the importance of utilizing multiparametric MRI for more informative and integrated evaluation of renal conditions, as demonstrated in previous experimental[21,50] and clinical[51] studies.

Our study is associated with some limitations. First, calibration of the cuff did not consider in vivo factors, such as variation in renal artery size and vascular resistance, which may lead to inaccurate estimation of the degree of RAS. Nevertheless, graded renal ischemia was clearly achieved, as supported by the ASL-measured renal perfusion. Furthermore, measurements using the different techniques were all obtained at the same level of renal arterial obstruction. Rather than the precise degree of obstruction, our study focused on comparing the sensitivity of these techniques to similar changes in renal perfusion pressure. Yet, a ~70% fall in renal perfusion at ~75% stenosis is high compared with other large vessels like the iliac artery.[52] Pertinently, in the renal artery of pigs, renal blood flow (RBF) starts falling over a threshold of 42% of RAS, with a rapid drop in RBF when RAS reached 70%.[53] Therefore, the combination of underestimated degree of RAS and the unique properties of the pig renal artery might have contributed to this ostensible precipitous fall in RBF. Second, we measured in this study renal perfusion, rather than renal arterial flow, which can be achieved using phase contrast MR or Doppler sonography.[54] Third, no control group was included in this study. However, our previous study using the same pig model has shown no change in renal parameters throughout the experimental period.[15] Furthermore, the main goal of this study was to compare the changes in different MRI methods. Therefore, renal parameters at baseline can be used for comparison with other time points. Fourth, we cannot rule out the possibility that at the recovery phase the MTR was affected by tissue edema. Fifth, although we have demonstrated that renal MTR is not affected by perfusion changes, other factors present in a fibrotic kidney, such as tubular atrophy, tissue edema, accumulation of other extracellular proteins, or inflammatory cell infiltration, may alter the measured MTR and thus compromise its specificity for renal fibrosis. Although we have previously shown that MTR measured in vitro in a collagen phantom at 16.4 T or 3 T correlates directly with collagen concentrations,[20,22] future studies are needed to investigate the impact of in vivo factors on renal MTR. Lastly, additional novel techniques for assessment of renal fibrosis with molecular MRI have not been tested.

In summary, MRI techniques useful for assessment of renal fibrosis have different susceptibility to acute alterations in renal perfusion. In swine kidneys with acute ischemia, renal ADC by DWI and stiffness by MRE substantially decrease without evidence of renal fibrosis, indicating their dependence on renal hemodynamics. By contrast, MTI is relatively insensitive to an acute decrease in renal perfusion and may offer a relatively reliable MRI technique for measurement of renal structural changes.

REFERENCES

1. United States Renal Data System. *2016 USRDS Annual Data Report: Epidemiology of Kidney Disease in the United States*. Bethesda, MD: National Institutes of Health, National Institute of Diabetes and Digestive and Kidney Diseases; 2016.
2. Khwaja A, El Kossi M, Floege J, et al. The management of CKD: a look into the future. *Kidney Int*. 2007;72:1316–1323.
3. Whittier WL, Korbet SM. Timing of complications in percutaneous renal biopsy. *J Am Soc Nephrol*. 2004;15:142–147.
4. Wells RG. Tissue mechanics and fibrosis. *Biochim Biophys Acta*. 2013;1832:884–890.
5. Conway B, Hughes J. Cellular orchestrators of renal fibrosis. *QJM*. 2012;105:611–615.
6. Togao O, Doi S, Kuro-o M, et al. Assessment of renal fibrosis with diffusion-weighted MR imaging: study with murine model of unilateral ureteral obstruction. *Radiology*. 2010;255:772–780.
7. Woo S, Cho JY, Kim SY, et al. Intravoxel incoherent motion MRI-derived parameters and T2* relaxation time for noninvasive assessment of renal fibrosis: an experimental study in a rabbit model of unilateral ureter obstruction. *Magn Reson Imaging*. 2018;51:104–112.
8. Friedli I, Crowe LA, Berchtold L, et al. New magnetic resonance imaging index for renal fibrosis assessment: a comparison between diffusion-weighted imaging and T1 mapping with histological validation. *Sci Rep*. 2016;6:30088.
9. Hueper K, Hensen B, Gutberlet M, et al. Kidney transplantation: multiparametric functional magnetic resonance imaging for assessment of renal allograft pathophysiology in mice. *Invest Radiol*. 2016;51:58–65.
10. Inoue T, Kozawa E, Okada H, et al. Noninvasive evaluation of kidney hypoxia and fibrosis using magnetic resonance imaging. *J Am Soc Nephrol*. 2011;22:1429–1434.
11. Zhao J, Wang ZJ, Liu M, et al. Assessment of renal fibrosis in chronic kidney disease using diffusion-weighted MRI. *Clin Radiol*. 2014;69:1117–1122.
12. Xu X, Palmer SL, Lin X, et al. Diffusion-weighted imaging and pathology of chronic kidney disease: initial study. *Abdom Radiol (NY)*. 2018;43:1749–1755.
13. Ebrahimi B, Rihal N, Woollard JR, et al. Assessment of renal artery stenosis using intravoxel incoherent motion diffusion-weighted magnetic resonance imaging analysis. *Invest Radiol*. 2014;49:640–646.
14. van Baalen S, Leemans A, Dik P, et al. Intravoxel incoherent motion modeling in the kidneys: comparison of mono-, bi-, and triexponential fit. *J Magn Reson Imaging*. 2017;46:228–239.
15. Warner L, Yin M, Glaser KJ, et al. Noninvasive In vivo assessment of renal tissue elasticity during graded renal ischemia using MR elastography. *Invest Radiol*. 2011;46:509–514.
16. Korsmo MJ, Ebrahimi B, Eirin A, et al. Magnetic resonance elastography noninvasively detects in vivo renal medullary fibrosis secondary to swine renal artery stenosis. *Invest Radiol*. 2013;48:61–68.
17. Gennisson JL, Grenier N, Combe C, et al. Supersonic shear wave elastography of in vivo pig kidney: influence of blood pressure, urinary pressure and tissue anisotropy. *Ultrasound Med Biol*. 2012;38:1559–1567.
18. Wolff SD, Balaban RS. Magnetization transfer imaging: practical aspects and clinical applications. *Radiology*. 1994;192:593–599.
19. Kline TL, Irazabal MV, Ebrahimi B, et al. Utilizing magnetization transfer imaging to investigate tissue remodeling in a murine model of autosomal dominant polycystic kidney disease. *Magn Reson Med*. 2016;75:1466–1473.
20. Jiang K, Ferguson CM, Ebrahimi B, et al. Noninvasive assessment of renal fibrosis with magnetization transfer MR imaging: validation and evaluation in murine renal artery stenosis. *Radiology*. 2017;283:77–86.
21. Jiang K, Ponzo TA, Tang H, et al. Multiparametric MRI detects longitudinal evolution of folic acid-induced nephropathy in mice. *Am J Physiol Renal Physiol*. 2018;315:F1252–F1260.
22. Jiang K, Ferguson CM, Woollard JR, et al. Magnetization transfer magnetic resonance imaging noninvasively detects renal fibrosis in swine atherosclerotic renal artery stenosis at 3.0 T. *Invest Radiol*. 2017;52:686–692.
23. Zun Z, Wong EC, Nayak KS. Assessment of myocardial blood flow (MBF) in humans using arterial spin labeling (ASL): feasibility and noise analysis. *Magn Reson Med*. 2009;62:975–983.
24. Martirosian P, Klose U, Mader I, et al. FAIR true-FISP perfusion imaging of the kidneys. *Magn Reson Med*. 2004;51:353–361.
25. Fenchel M, Martirosian P, Langanke J, et al. Perfusion MR imaging with FAIR true FISP spin labeling in patients with and without renal artery stenosis: initial experience. *Radiology*. 2006;238:1013–1021.
26. Le Bihan D, Breton E, Lallemand D, et al. Separation of diffusion and perfusion in intravoxel incoherent motion MR imaging. *Radiology*. 1988;168:497–505.
27. Silva AM, Grimm RC, Glaser KJ, et al. Magnetic resonance elastography: evaluation of new inversion algorithm and quantitative analysis method. *Abdom Imaging*. 2015;40:810–817.
28. Yin M, Glaser KJ, Talwalkar JA, et al. Hepatic MR elastography: clinical performance in a series of 1377 consecutive examinations. *Radiology*. 2016;278:114–124.
29. Wolf M, de Boer A, Sharma K, et al. Magnetic resonance imaging T1- and T2-mapping to assess renal structure and function: a systematic review and statement paper. *Nephrol Dial Transplant*. 2018;33(suppl_2):ii41–ii50.
30. Schainuck LI, Striker GE, Cutler RE, et al. Structural-functional correlations in renal disease. II. The correlations. *Hum Pathol*. 1970;1:631–641.
31. Farris AB, Adams CD, Brousaides N, et al. Morphometric and visual evaluation of fibrosis in renal biopsies. *J Am Soc Nephrol*. 2011;22:176–186.
32. Risdon RA, Sloper JC, De Wardener HE. Relationship between renal function and histological changes found in renal-biopsy specimens from patients with persistent glomerular nephritis. *Lancet*. 1968;2:363–366.

33. Roberts IS, Cook HT, Troyanov S, et al. The Oxford classification of IgA nephropathy: pathology definitions, correlations, and reproducibility. *Kidney Int*. 2009;76:546–556.
34. Grimm PC, Nickerson P, Gough J, et al. Quantitation of allograft fibrosis and chronic allograft nephropathy. *Pediatr Transplant*. 1999;3:257–270.
35. Choi BS, Shin MJ, Shin SJ, et al. Clinical significance of an early protocol biopsy in living-donor renal transplantation: ten-year experience at a single center. *Am J Transplant*. 2005;5:1354–1360.
36. Cosio FG, Grande JP, Wadei H, et al. Predicting subsequent decline in kidney allograft function from early surveillance biopsies. *Am J Transplant*. 2005;5:2464–2472.
37. Fleig SV, Humphreys BD. Rationale of mesenchymal stem cell therapy in kidney injury. *Nephron Clin Pract*. 2014;127:75–80.
38. Hickson LJ, Eirin A, Lerman LO. Challenges and opportunities for stem cell therapy in patients with chronic kidney disease. *Kidney Int*. 2016;89:767–778.
39. Zou X, Kwon SH, Jiang K, et al. Renal scattered tubular-like cells confer protective effects in the stenotic murine kidney mediated by release of extracellular vesicles. *Sci Rep*. 2018;8:1263.
40. Zou X, Jiang K, Puranik AS, et al. Targeting murine mesenchymal stem cells to kidney injury molecule-1 improves their therapeutic efficacy in chronic ischemic kidney injury. *Stem Cells Transl Med*. 2018;7:394–403.
41. Prasad PV, Li LP, Thacker JM, et al. Cortical perfusion and tubular function as evaluated by magnetic resonance imaging correlates with annual loss in renal function in moderate chronic kidney disease. *Am J Nephrol*. 2019;49:114–124.
42. Storey P, Ji L, Li LP, et al. Sensitivity of USPIO-enhanced R2 imaging to dynamic blood volume changes in the rat kidney. *J Magn Reson Imaging*. 2011;33:1091–1099.
43. Boor P, Perkuhn M, Weibrecht M, et al. Diffusion-weighted MRI does not reflect kidney fibrosis in a rat model of fibrosis. *J Magn Reson Imaging*. 2015;42:990–998.
44. Ebrahimi B, Saad A, Jiang K, et al. Renal adiposity confounds quantitative assessment of markers of renal diffusion with MRI: a proposed correction method. *Invest Radiol*. 2017;52:672–679.
45. Marticorena Garcia SR, Grossmann M, Bruns A, et al. Tomoelastography paired with T2* magnetic resonance imaging detects lupus nephritis with normal renal function. *Invest Radiol*. 2019;54:89–97.
46. Asano K, Ogata A, Tanaka K, et al. Acoustic radiation force impulse elastography of the kidneys: is shear wave velocity affected by tissue fibrosis or renal blood flow? *J Ultrasound Med*. 2014;33:793–801.
47. Wang HK, Lai YC, Lin YH, et al. Acoustic radiation force impulse imaging of the transplant kidney: correlation between cortical stiffness and arterial resistance in early post-transplant period. *Transplant Proc*. 2017;49:1001–1004.
48. Basile DP, Anderson MD, Sutton TA. Pathophysiology of acute kidney injury. *Compr Physiol*. 2012;2:1303–1353.
49. Walker PD. Alterations in renal tubular extracellular matrix components after ischemia-reperfusion injury to the kidney. *Lab Invest*. 1994;70:339–345.
50. Wang F, Takahashi K, Li H, et al. Assessment of unilateral ureter obstruction with multi-parametric MRI. *Magn Reson Med*. 2018;79:2216–2227.
51. Prasad PV, Thacker J, Li LP, et al. Multi-parametric evaluation of chronic kidney disease by MRI: a preliminary cross-sectional study. *PLoS One*. 2015;10:e0139661.
52. Levin DC, Beckmann CF, Serur JR. Vascular resistance changes distal to progressive arterial stenosis: a critical re-evaluation of the concept of vasodilator reserve. *Invest Radiol*. 1980;15:120–128.
53. Rognant N, Rouviere O, Janier M, et al. Hemodynamic responses to acute and gradual renal artery stenosis in pigs. *Am J Hypertens*. 2010;23:1216–1219.
54. Schoenberg SO, Knopp MV, Bock M, et al. Renal artery stenosis: grading of hemodynamic changes with cine phase-contrast MR blood flow measurements. *Radiology*. 1997;203:45–53.